(Received 23 November 2025, Accepted 4 January 2026, Scheduled 8 February 2026)

Design of Compact Spiral Antenna with Modified Feed Structure for Electronic Warfare Applications

Abhay M. Morey[1, *], Avinash R. Vaidya[1], and Sandeepak S. Kakatkar[2]

[1] *Department of Electronics Engineering, Pillai College of Engineering,New Panvel, University of Mumbai, Mumbai 410206, India*
[2] *Society for Applied Microwave Electronics Engineering and Research, Mumbai 400076, India*

ABSTRACT: This paper proposes a compact spiral antenna with a reduced profile, achieved by integrating a modified tapered balun feed structure with reflector backing. The proposed configuration introduces sharp bends in the tapered balun, significantly reducing the antenna height without degrading broadband performance. Experimental results demonstrate stable impedance matching and preservation of circular polarization over a wide frequency range of 2–18 GHz. The measured radiation performance indicated negligible degradation in radiation loss, impedance continuity, polarization purity, and bandwidth compared to a conventional configuration. The proposed approach validated the practical feasibility of incorporating sharp bends in tapered baluns for spiral antennas, enabling low-profile integration in space-constrained platforms. Due to its compact size and robust radiation characteristics, the antenna was well-suited for electronic countermeasure (ECM) applications, including radar warning receivers, missile systems, and electronic warfare pods.

1. INTRODUCTION

Electronic warfare applications require compact, lightweight antennas with wideband characteristics. Frequency-independent antennas are well known for maintaining stable impedance matching, gain, and radiation patterns over a broad frequency range. Among them, spiral antenna is one of the most suitable candidates for circular polarization. The wavelength corresponding to the lowest operating frequency determines the overall size of the spiral antenna; consequently, at lower frequencies, the antenna size increases [1]. Spiral antennas inherently exhibit bidirectional radiation, and therefore, a conductive backing cavity is commonly employed to suppress back radiation and achieve unidirectional radiation [2].

In recent years, compact antenna designs have attracted considerable attention. Compact slot spiral antennas have been developed, with the balun typically positioned on the backside of the slot structure [3]. A horizontal L-shaped balun was introduced to reduce the antenna profile [4]. Several antenna size-reduction techniques have been reported, including ring loading, tapered arm terminations, meander-line peripheries, and resistive arm terminations [5]. A coplanar waveguide (CPW) feed has also been employed to eliminate the need for an external balun, thereby enhancing antenna compactness [6]. Koch curves have been utilized for spiral antenna miniaturization, achieving a size reduction of up to 49% [7]. Further size reduction has been realized using extended arms and lumped resistors, whereas circular polarization performance has been improved through the use of a cross-slot reflector [8]. Wideband feeding was achieved using a 1.14 mm twin-line transmission line through a microstrip-to-parallel-strip transition, providing efficient impedance matching [9]. Modified tapered microstrip baluns with U-shaped configurations have been reported to reduce the feed length at the expense of increasing width [10]. However, antenna performance has been shown to degrade with even minor bending of the balun, resulting in deterioration of balanced-mode operation, return loss, radiation pattern, circular polarization, and CP beamwidth across the operating band [11].

In this study, a novel compact spiral antenna incorporating a 90° bend in the feed structure was investigated for operation over the 2–18 GHz frequency range. The proposed design demonstrates significant improvements in gain, impedance matching, and axial ratio (AR) performance compared with a conventional straight-balun-fed spiral antenna. Furthermore, the integration of the modified feed with a ground backing leads to a substantial reduction in the antenna size, which is essential for applications requiring compact and adaptable configurations. Despite the reduced size, the antenna maintains excellent broadband performance while minimizing spatial requirements.

2. DESIGN OF THE ANTENNA

2.1. Spiral Antenna Design

The centerline of the spiral antenna is governed by the Archimedean function [12], with spiral geometry as shown in Fig. 1.

$$r_{\text{sp}} = a_{\text{sp}} \cdot \varphi_w \tag{1}$$

where r_{sp} is the radius of the spiral measured from the origin to the centerline of the arm; $a_{\text{sp}} = 1.273\,\text{mm/rad}$ is the spiral constant; and φ_w is the winding angle.

* Corresponding author: Abhay M. Morey (mabhay22phd@student.mes.ac.in).

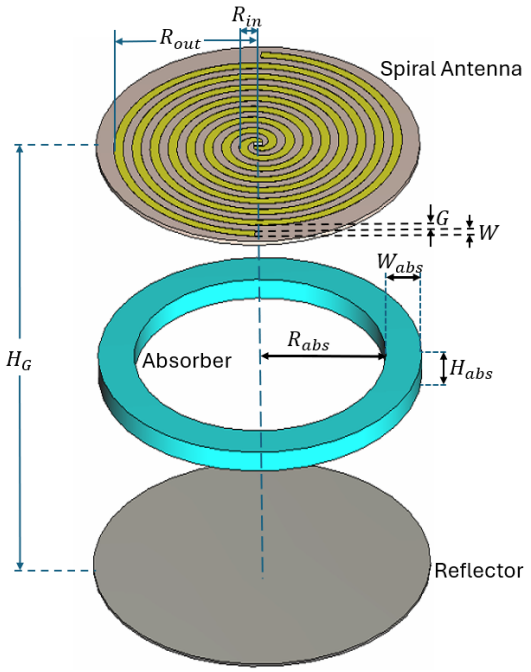

FIGURE 1. Schematic of the spiral antenna with absorber and reflector backing.

The operating frequency of the spiral antenna was determined using (2) and (3) [12].

$$R_{\text{out}} \geq \frac{c}{2\pi F_L \sqrt{\epsilon_{\text{eff}}}} \tag{2}$$

$$R_{\text{in}} \leq \frac{c}{2\pi F_H \sqrt{\epsilon_{\text{eff}}}} \tag{3}$$

where R_{in} and R_{out} denote the inner and outer radii of the spiral, respectively; ϵ_{eff} is the effective dielectric constant; F_L and F_H are the lowest and highest operating frequencies, respectively; and the number of turns N is defined as [12]

$$N = \frac{R_{\text{out}} - R_{\text{in}}}{4W} \tag{4}$$

An eight-turn spiral antenna with an arm width (W) and spacing (G) of 2.0 mm was fabricated on a Rogers RT/duroid 5880 substrate with a thickness of 0.8 mm ($\varepsilon_r = 2.2$, $\tan\delta = 0.0009$). A JVMBF226 flat absorber [22] ($\varepsilon' = 49.5$, $\varepsilon'' = 1.15$, $\mu' = 1.9$, and $\mu'' = 2.3$ at 10 GHz) with a height (H_{abs}) of 5 mm, a width (W_{abs}) of 10 mm, and an inner radius (R_{abs}) of 30 mm was placed beneath the antenna to enhance the low-frequency performance. The designed structure was simulated using Dassault Systèmes' CST Microwave Studio Suite 2021 [23] with a time-domain solver and adaptive hexahedral mesh. The mesh was automatically refined based on energy and field convergence criteria, ensuring a minimum of 25 cells per wavelength at the lowest operating frequency of 2 GHz. Additional local mesh refinement was applied in the feed transition and tapered balun regions to accurately capture rapid field variations. Open boundary conditions with approximately one-quarter-wavelength padding were used in all directions to emulate free-space radiation and to suppress spurious reflections.

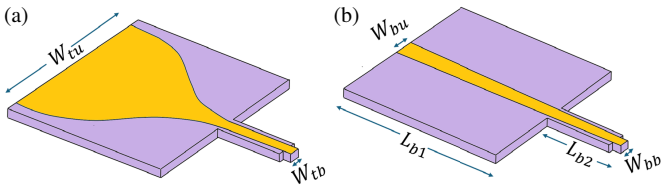

FIGURE 2. Structure of straight tapered feed balun. (a) Top side. (b) Bottom side.

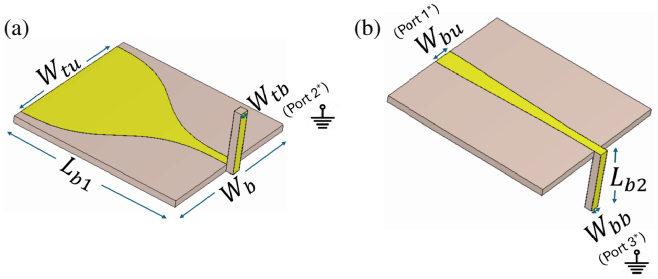

FIGURE 3. Structure of modified tapered feed balun. (a) Top side. (b) Bottom side. (* CMRR simulation port representation in CST).

2.2. Modified Tapered Microstrip Balun

Spiral antennas require a balun to provide a transition between their balanced structure and unbalanced coaxial feed, thereby preventing tilted current distributions caused by unequal currents in the spiral arms. A spiral geometry printed on a dielectric substrate exhibits an impedance of approximately 120 Ω across the operating band, which would otherwise result in poor impedance matching when directly connected to standard microwave equipment, typically characterized by a 50 Ω impedance [1]. Accordingly, the balun was designed to match the unbalanced microstrip line to the balanced spiral using tapered transitions and microstrip-to-parallel-line principles [20]. The balun was implemented on a Rogers RT/Duroid 5880 substrate ($\varepsilon_r = 2.2$, $\tan\delta = 0.0009$) with a thickness of 1.57 mm. Fig. 2 illustrates the straight balun configuration, which was subsequently modified by introducing a bend at the required location. The top and bottom views of the modified tapered feed balun are shown in Figs. 3(a) and (b), respectively.

The width (W_{tu}) and total length ($L_b = L_{b1} + L_{b2}$) of the unbalanced section were optimized to maintain balun balance, which was quantitatively evaluated using the common-mode rejection ratio (CMRR) [21].

$$\text{CMRR} = 20 \cdot \log_{10} \frac{A_{\text{dm}}}{A_{\text{cm}}} \tag{5}$$

where A_{dm} is the differential mode transmission coefficient, and A_{cm} is the common mode transmission coefficient of the balun.

$$A_{\text{dm}} = A - B\angle\Delta\phi \tag{6}$$

$$A_{\text{cm}} = A + B\angle\Delta\phi \tag{7}$$

where A and B represent the complex field values received by the top and bottom strips at the balanced side, respectively, with a phase difference of $\angle\Delta\phi$. Ideally, the field magnitudes at both balanced strips should be equal to 180° out of phase, i.e.,

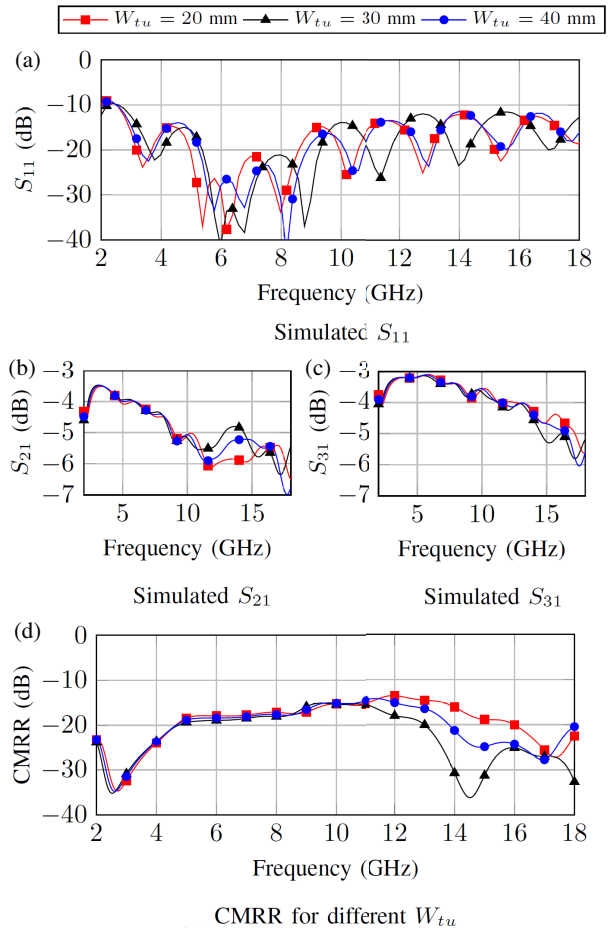

FIGURE 4. Simulated (a) $|S_{11}|$, (b) $|S_{21}|$, (c) $|S_{31}|$, and (d) CMRR with varying W_{tu}.

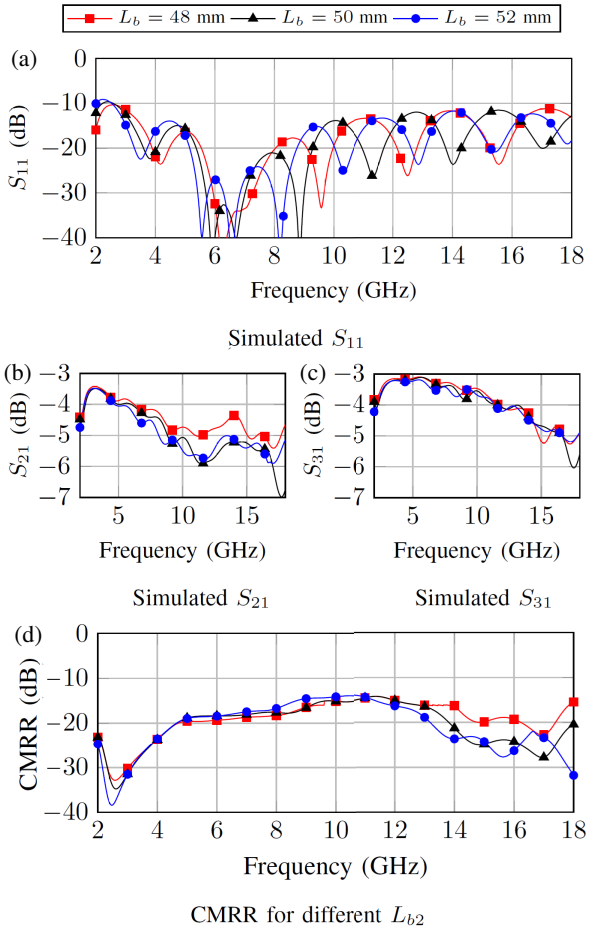

FIGURE 5. Simulated (a) $|S_{11}|$, (b) $|S_{21}|$, (c) $|S_{31}|$, and (d) CMRR with varying L_b.

$A = B$ and $\angle\Delta\phi = 180°$. Under these conditions, the structure exhibits a low common-mode rejection ratio (CMRR). In CST Studio Suite, Ports 2 and 3 are assigned to the top and bottom strips at the balanced side, whereas Port 1 is connected to the unbalanced side as shown in Fig. 3. The simulated S-parameters are obtained by varying W_{tu} to 20 mm, 30 mm, and 40 mm, as shown in Figs. 4(a), (b), and (c). In all cases, good impedance matching and an equal power distribution between the balanced ports were observed. The corresponding CMRR was plotted in Fig. 4(d), where the minimum CMRR is achieved for $W_{tu} = 30$ mm. This confirms that the balun effectively generates balanced signals, resulting in an excellent CMRR performance.

Similarly, to investigate the effect of balun length ($L_b = L_{b1} + L_{b2}$), L_b was varied to 48 mm, 50 mm, and 52 mm. The corresponding S-parameters are plotted in Figs. 5(a), (b), and (c), and the CMRR is shown in Fig. 5(d). A minimum CMRR was observed for $L_b = 52$ mm, indicating improved balun balance at this length.

2.3. Reflector Backing Integrated Modified Balun

Subsequently, the ground plane of the modified feed was integrated into the substrate, serving as both the signal reference and reflective backing. This integration enhances the overall antenna performance while significantly reducing the antenna size. The gap B_G between the balun and reflector ground is optimized in the following section to achieve a lower insertion loss, improved return loss, and a controlled current distribution. The top view of the integrated structure is shown in Fig. 6(a), while Fig. 6(b) illustrates the microstrip line on the bottom layer of the substrate carrying the unbalanced input signal, Fig. 6(c)

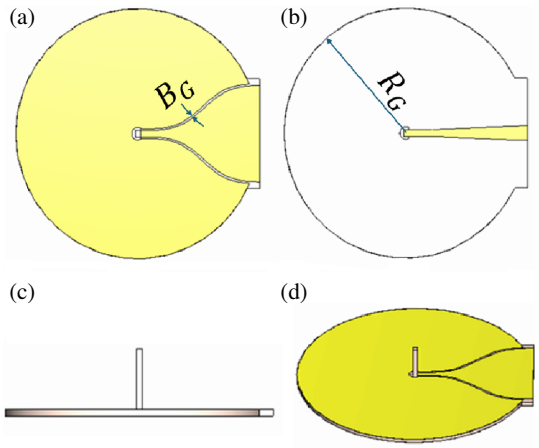

FIGURE 6. Modified integrated ground feed with reflector backing. (a) Top view. (b) Bottom view. (c) Side view. (d) Isometric view.

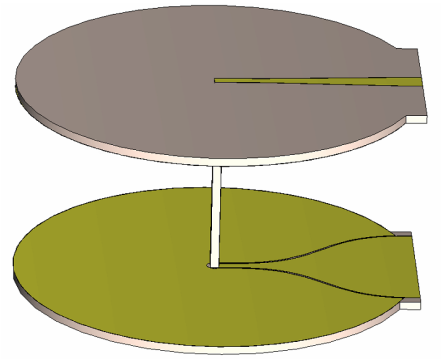

FIGURE 7. Simulated modified ground integrated balun in back-to-back configuration.

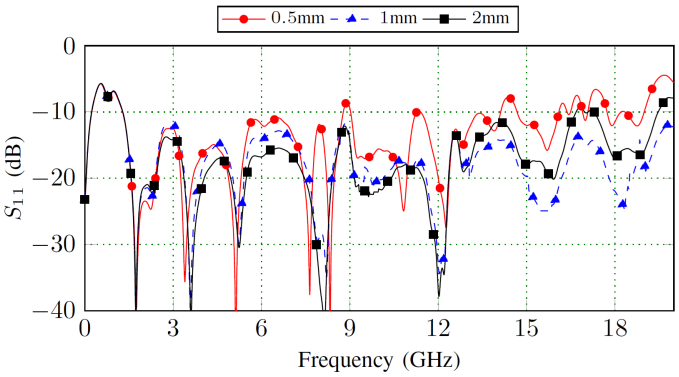

FIGURE 8. Simulated S_{11} of balun with B_G gap variation.

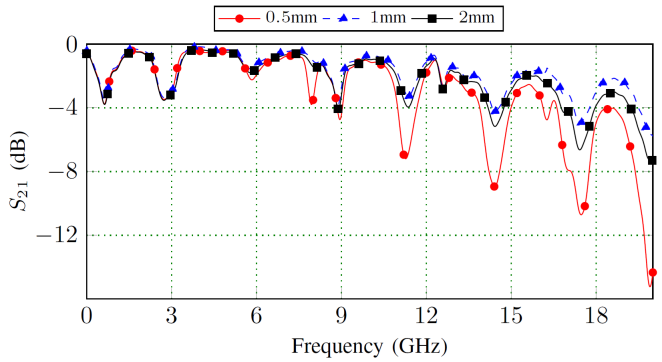

FIGURE 9. Simulated S_{21} of balun with B_G gap variation.

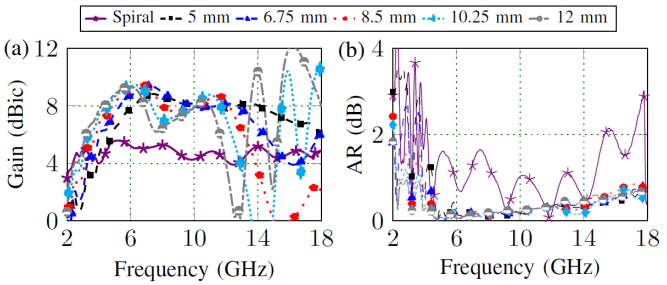

FIGURE 10. Parametric study by varying the height of the ground reflector. (a) Gain. (b) Axial Ratio (AR).

presents a side view; and Fig. 6(d) provides an isometric view of the designed balun structure. Using this modified structure, we reduced the antenna height by approximately 55–60%.

A detailed parametric study was carried out to investigate the effect of the gap width (B_G) between the balun ground and reflector ground in a back-to-back configuration, as illustrated in Fig. 7. The balun performance was simulated for three different gap widths, namely $B_G = 0.5$ mm, 1 mm, and 2 mm, over the 0–20 GHz frequency range to assess their impact on impedance matching, insertion loss, and overall compactness.

The return loss ($|S_{11}|$), shown in Fig. 8, indicates that all three configurations exhibit good impedance matching across the operating band, with $|S_{11}|$ remaining below -10 dB. Among them, the case with $B_G = 1$ mm provided superior matching, particularly at lower frequencies. This behavior suggests that the selected gap width enables optimal electromagnetic coupling between the balun and reflector ground, resulting in a smoother current transition and improved impedance transformation.

The insertion loss ($|S_{21}|$), shown in Fig. 9, further highlights the dependence on the gap width. A narrower gap of 0.5 mm results in slightly higher insertion loss owing to increased capacitive coupling and stronger signal confinement, whereas a wider gap of 2 mm reduces the insertion loss. Compared to the intermediate case of $B_G = 1$ mm, this provides an optimal trade-off, achieving low insertion loss while maintaining compactness.

Overall, the comparative analysis of $|S_{11}|$ and $|S_{21}|$ confirms that a 1 mm gap between the balun ground and the reflector ground yields the most optimized performance, providing lower insertion loss, improved return loss, and well-controlled current distribution.

2.4. Reflector Spacing Variation

The influence of the reflector spacing H_G on the gain and axial ratio (AR) of the spiral antenna, together with the phase interaction between the direct and reflected fields, was shown in Fig. 10. To isolate the intrinsic radiation behavior, the spiral is excited using an absorber ring and a backing reflector only, without the balun, ensuring symmetric excitation and suppression of higher-order mode leakage.

At lower frequencies (2–8 GHz), the active region of the spiral lies toward the outer turns, resulting in a small electrical spacing from the reflector ($\ll \lambda/4$). Consequently, the reflected field remains approximately in phase with the direct radiation, producing constructive interference and a stable gain and axial ratio (AR) for all reflector spacings, as shown in Figs. 10(a) and (b). As the frequency increases, the active region progressively migrates inward, thereby increasing its electrical spacing from the reflector. For a fixed spacing of 12 mm, this separation approaches approximately $\lambda/2$ near 12–13 GHz, causing the reflected field to become nearly 180° out of phase with the direct field. This phase reversal results in the observed gain dip around 12.5 GHz and a corresponding degradation in the AR. A reflector-spacing sweep from 5 to 12 mm further

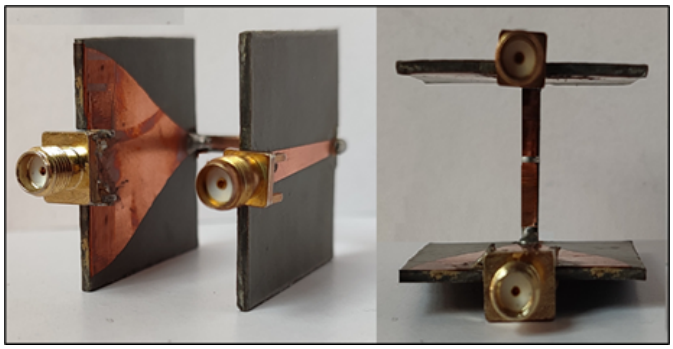

FIGURE 11. Fabricated modified balun in back-to-back configuration.

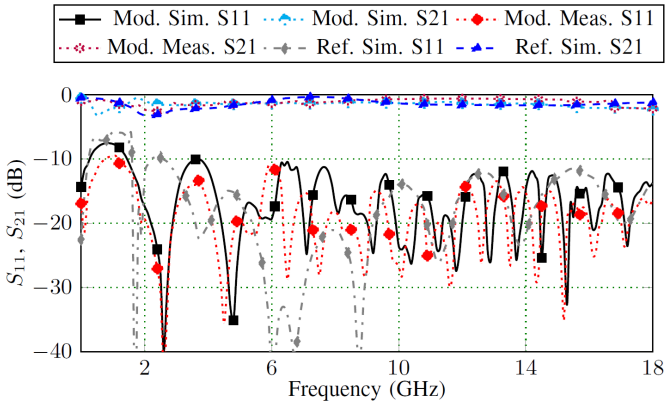

FIGURE 12. Simulated and measured S-parameters of modified balun in back-to-back configuration.

confirms that smaller spacings maintain an electrical separation of less than $\lambda/4$ over most of the operating band, leading to a smoother gain variation and consistently low AR. By contrast, larger spacings introduce pronounced high-frequency gain fluctuations owing to the increased phase mismatch between the direct and reflected fields. These observations highlight the inherent trade-off associated with fixed reflector spacing in wideband spiral antennas and motivate the need for spacing optimization or absorber loading to stabilize the broadband performance.

3. EXPERIMENTAL VALIDATION

3.1. Fabricated Prototype of Modified Feed

The balun was designed with a primary length of $L_{b1} = 40\,\text{mm}$, which is equal to the radius of the spiral antenna, and a secondary length of $L_{b2} = 12\,\text{mm}$. The overall balun width was maintained at $W_b = 33\,\text{mm}$, whereas the top-plane width ($W_{tu} = 30\,\text{mm}$) and bottom-plane width ($W_{bu} = 4.5\,\text{mm}$) at the input end were selected to provide a characteristic impedance of approximately $50\,\Omega$, which is suitable for the unbalanced coaxial feed. These widths gradually taper to $W_{tb} = W_{bb} = 2.1\,\text{mm}$ at the output end to form a balanced transmission line with an impedance of approximately $120\,\Omega$, matching the input of the spiral antenna. Parallel trace lines were maintained over a combined length of $L_{b1} + L_{b2} = 52\,\text{mm}$. A photograph of the fabricated modified balun in back-to-back configuration is shown in Fig. 11.

FIGURE 13. Fabricated modified balun with spiral antenna.

The matching and losses were measured by connecting two unbalanced ports to a calibrated Vector Network Analyzer (VNA). The simulated and measured S-parameters for both the proposed modified balun and conventional straight balun (used as a reference) are summarized in Fig. 12. The modified balun demonstrates enhanced broadband performance, with simulated and measured $|S_{11}|$ values closely aligned and consistently below $-10\,\text{dB}$ across the 2–18 GHz range, indicating good impedance matching. The transmission coefficient, $|S_{21}|$, remained close to 0 dB in all cases, confirming minimal insertion loss and negligible inter-port coupling. These results validate the effectiveness of the proposed balun in achieving wideband impedance matching while maintaining low transmission loss.

3.2. Fabricated Prototype of Antenna with Modified Feed

The antenna was placed over a carefully fabricated modified feed balun, as shown in Fig. 13. Measurements were conducted using a Keysight FieldFox N9917A vector network analyzer (VNA) with standard SOLT calibration to minimize systematic errors. The measured and simulated results for the proposed antenna are shown in Fig. 14. As shown in Fig. 14(a), the antenna with the modified feed balun achieves wideband impedance matching, with $|S_{11}| < -10\,\text{dB}$ across the entire 2–18 GHz frequency range. For a comparative analysis, an antenna integrated with a straight balun was used as a reference, providing a benchmark for evaluating the improvements in return loss, bandwidth, and compactness achieved by the proposed design.

The measured S_{11} exhibits minor deviations from the simulated response, primarily because of the practical 90° balun transition formed by soldering the top and bottom traces, which introduces parasitic inductance and slight asymmetry that is not accounted for in the idealized model. Additional discrepancies arise from parasitic effects associated with the SMA-to-balun launch and the soldered balun-to-antenna interface, as well as fabrication tolerances wideband measurement uncertainties. Overall, the measured S_{11} remains below $-10\,\text{dB}$ over the same bandwidth as the simulation, thereby validating the proposed design.

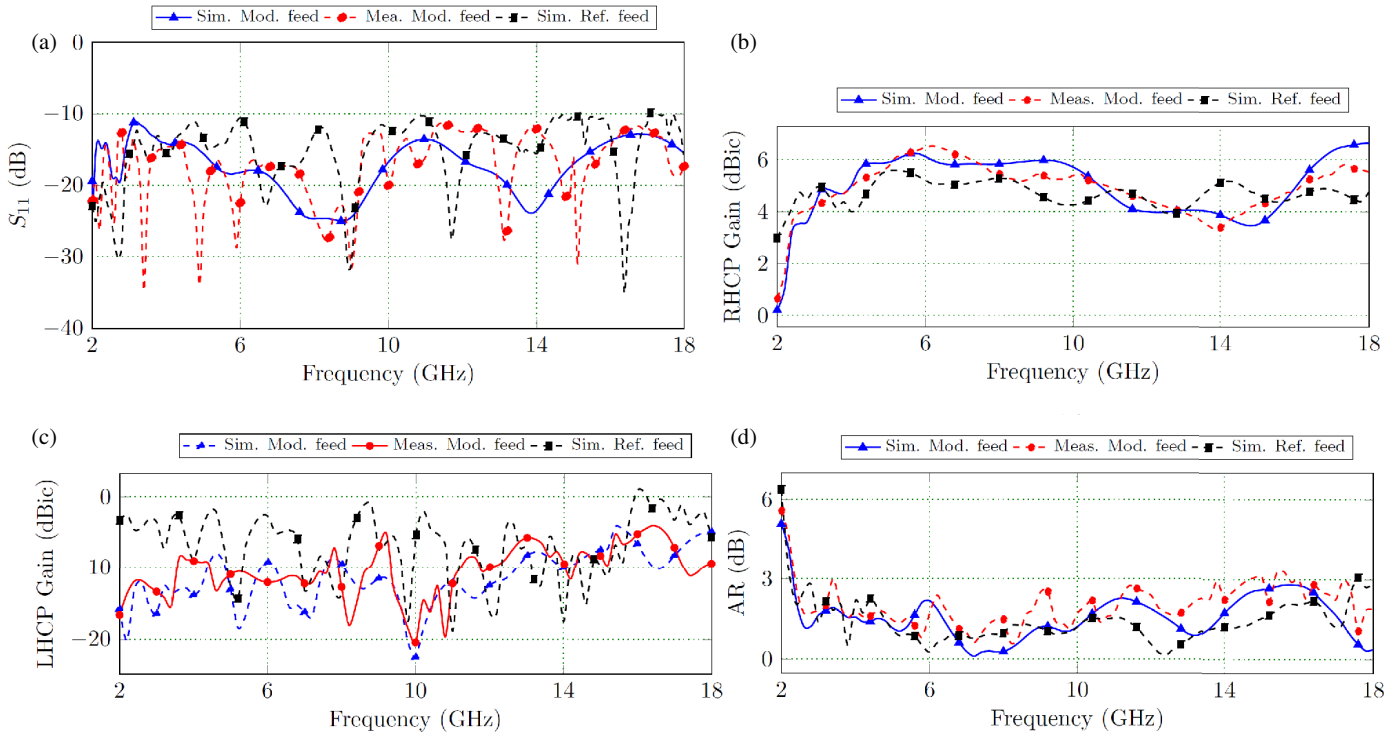

FIGURE 14. Simulated and measured (a) $|S_{11}|$, (b) RHCP gain, (c) LHCP gain, and (d) axial ratio (AR) of the proposed modified balun antenna.

Absolute gain measurements were conducted in an anechoic chamber using a calibrated horn antenna under far-field and co-polarized alignment. The dynamic range of the chamber exceeded 60 dB, allowing a reliable measurement of low-level cross-polarized components for accurate axial ratio (AR) evaluation. The losses from the balun and mounting fixtures are accounted for, and measurement uncertainty, including VNA calibration, reference antenna, chamber noise, and alignment effects, was estimated as ± 0.6 dB for gain and ± 0.5 dB for AR. Right-hand circular polarization (RHCP) and left-hand circular polarization (LHCP) gains were calculated from the measured linear response of the reference antenna. As shown in Fig. 14(b), the RHCP gain ranges from 0.5 to 6.2 dBic across 2–18 GHz, with the modified feed providing noticeably improved low-frequency gain and overall superior performance, despite a slight reduction around 14 GHz, the modified feed still delivers superior overall performance, confirming the effectiveness of the proposed balun structure. As shown in Fig. 14(c), the LHCP gain benefits from the balun bend acting as a partial reflector, ranging from -22 to -6.5 dBic across the band. The simulated and measured AR (Fig. 14(d)) remained below 3 dB over nearly the entire band for both the modified and reference feeds, with the modified feed showing fewer spikes and more consistent performance. These results confirm that the proposed feed enhances the radiation characteristics without compromising circular polarization.

3.3. Fabricated Modified Feed Integrated Backing Antenna

The fabricated spiral geometry is shown in Fig. 15(a). The fabricated spiral geometry is shown in Fig. 15(a). The absorber was placed 5 mm above the backing as shown in Fig. 15(b). Fig. 15(c) depicts the top layer of the balun integrated printed circuit board (PCB), whereas Fig. 15(d) presents the bottom layer of the modified balun. The antenna dimensions were 70 mm $\times$ 16 mm, excluding the 3D-printed packaging.

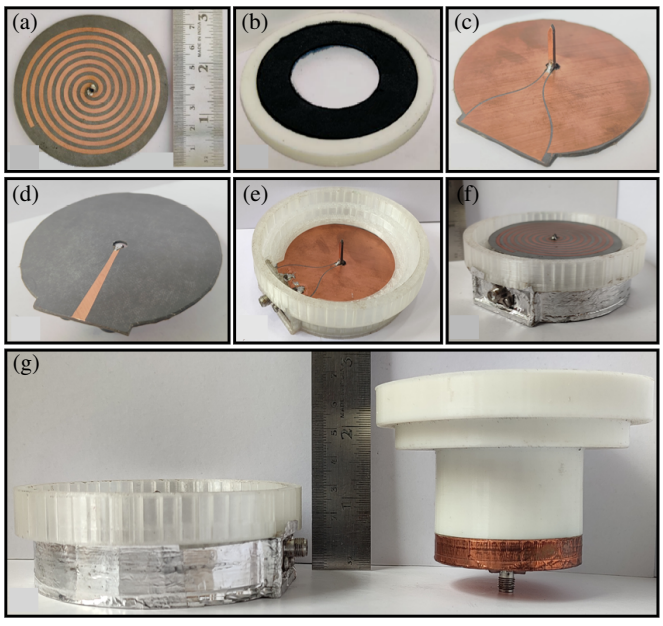

FIGURE 15. Fabricated prototype of antenna. (a) Spiral Antenna. (b) Absorber on support. (c) Balun integrated backing top side. (d) Balun integrated backing bottom side. (e) Balun integrated backing fitted inside the assembly housing. (f) Complete antenna assembly. (g) Comparison with the reference antenna.

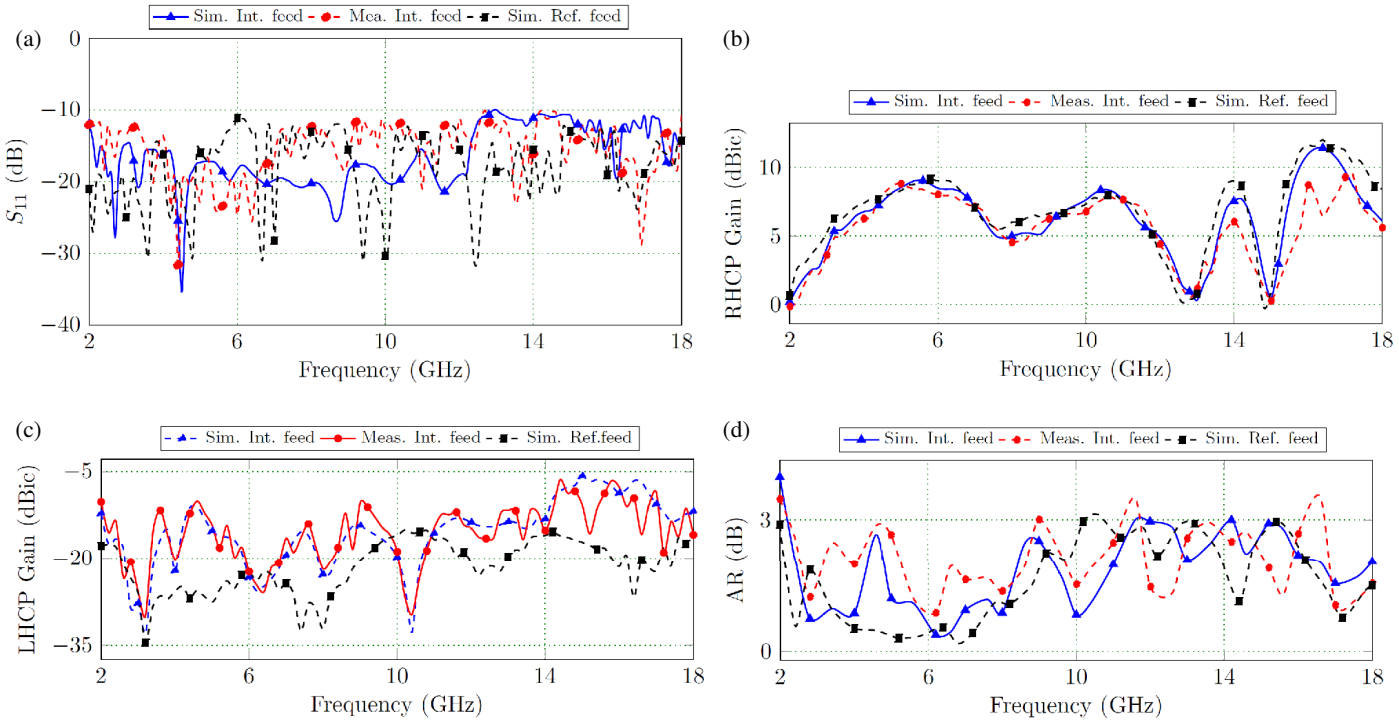

FIGURE 16. Simulated and measured (a) $|S_{11}|$, (b) RHCP gain, (c) LHCP gain, and (d) AR of the ground integrated modified balun antenna.

A balun PCB was installed in the antenna housing, as shown in Fig. 15(e). Antenna and modified integrated ground balun, together with the enclosure assemblies, are fitted as illustrated in Fig. 15(f). For a comparative analysis, a reference spiral antenna fed by a straight balun with a reflector spacing of 12 mm was employed. The total height was measured from the top of the spiral PCB to the bottom of the reflector, including all mechanical and electrical components. For the assembled prototypes with packaging, as shown in Fig. 15(g), the measured heights are 71 mm for the reference antenna ($H/\lambda \approx 0.47$ at 2 GHz) and 31 mm for the proposed antenna ($H/\lambda \approx 0.21$), corresponding to an approximately 55–60% reduction in profile height. When considering the electrical structure only, without packaging, the height reduction is even larger ($\sim$ 76%); however, this comparison focuses on packaged prototypes.

The reflector-integrated modified feed antenna was characterized using a Keysight FieldFox N9917A VNA. The measured reflection coefficient, $|S_{11}|$, remained below -10 dB across the entire 2–18 GHz band, as shown in Fig. 16(a). Fig. 16(b) shows the RHCP gain, ranging from 0.1 to 10 dBic. With a reflector spacing of 12 mm, noticeable dips in gain occurred, particularly near 12.5 GHz. This reduction arises because the reflector spacing approaches half of the free-space wavelength ($d \approx \lambda/2$) at this frequency, causing the reflected wave to be approximately 180° out of phase with direct radiation. The corresponding round-trip phase difference is given by $\phi = 4\pi d/\lambda$, illustrating the effect of reflector spacing on antenna gain. Fig. 16(c) shows the LHCP gain, which varies from -25 dBic to -5 dBic across the 2–18 GHz band. Fig. 16(d) presents both the simulated and measured axial ratios (ARs), which remain below 3 dB over most of the operating band (2.15–18 GHz), confirming effective circular polarization. Minor AR peaks coincide with dips in RHCP gain, indicating localized reductions in polarization purity.

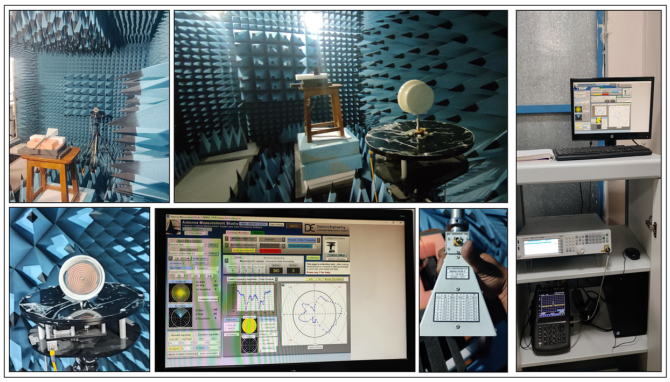

FIGURE 17. Radiation pattern measurement setup.

The radiation patterns of the antenna were measured in an anechoic chamber using the standard measurement setup shown in Fig. 17. A calibrated horn antenna served as the reference transmitter, and the antenna under test (AUT) was mounted on a motorized positioner to record radiation patterns in the $\phi = 0°$ and $\phi = 90°$ planes, as shown in Fig. 18. This setup enabled a reliable characterization of RHCP and LHCP components across the operating band. The LHCP levels are suppressed by more than 15–20 dB over most of the band, with noticeable polarization degradation and increased cross-polarization observed only at higher frequencies ($\geq$ 14 GHz), primarily due to reflector-induced phase imbalance.

Overall, the measured radiation patterns showed good agreement with the simulations, confirming the wideband circular

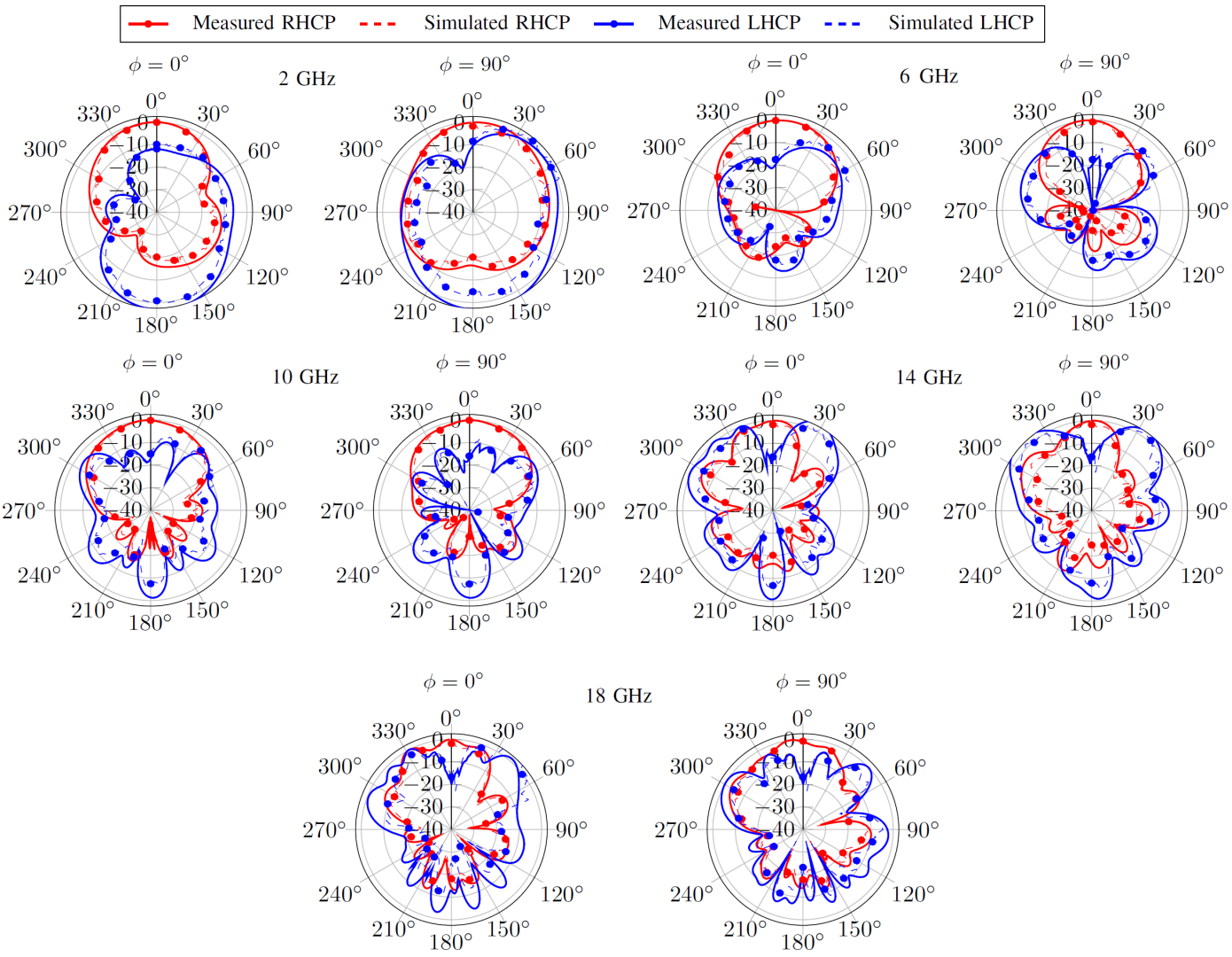

FIGURE 18. Normalized radiation patterns at $\phi = 0°$ and $\phi = 90°$ planes at different frequencies.

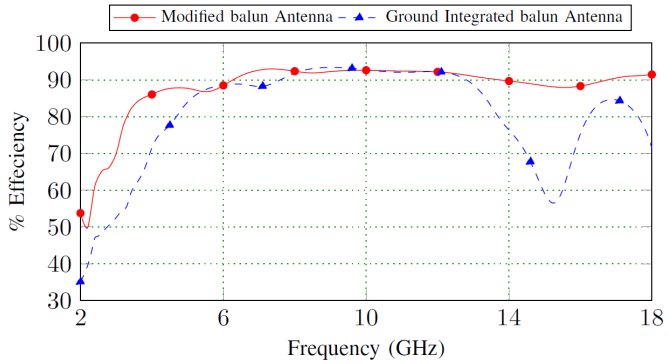

FIGURE 19. Simulated % effeciency of the proposed design.

polarization performance of the proposed antenna. Minor discrepancies can be attributed to fabrication tolerances in the tapered balun and feed structure, including connector transitions, solder joints, and slight mechanical deformations, which were not fully captured in the idealized CST model. Despite these effects, the main-beam direction, polarization sense, and frequency-dependent pattern behavior remain consistent with the simulated results.

The simulated radiation efficiency of the proposed spiral antenna with the modified balun and ground-integrated balun at 2–18 GHz is shown in Fig. 19. The modified balun antenna maintains high and stable efficiency ($\approx$ 50–90%) across the band, whereas the ground-integrated balun exhibits reduced efficiency, decreasing to approximately 35% at 2 GHz and 55% near 15 GHz owing to increased ground coupling and parasitic losses.

The axial ratio (AR) plots at $\phi = 0°$ and $\phi = 90°$ for different frequencies are shown in Fig. 20. At 2 GHz, the AR slightly exceeds 3 dB, whereas at all other frequencies, it remains within the 3 dB limit. The measured and simulated results follow the same trend and exhibit very close agreement across the operating band.

Table 1 summarizes the performance comparison with previous works; for a fair comparison, the antenna's electrical length

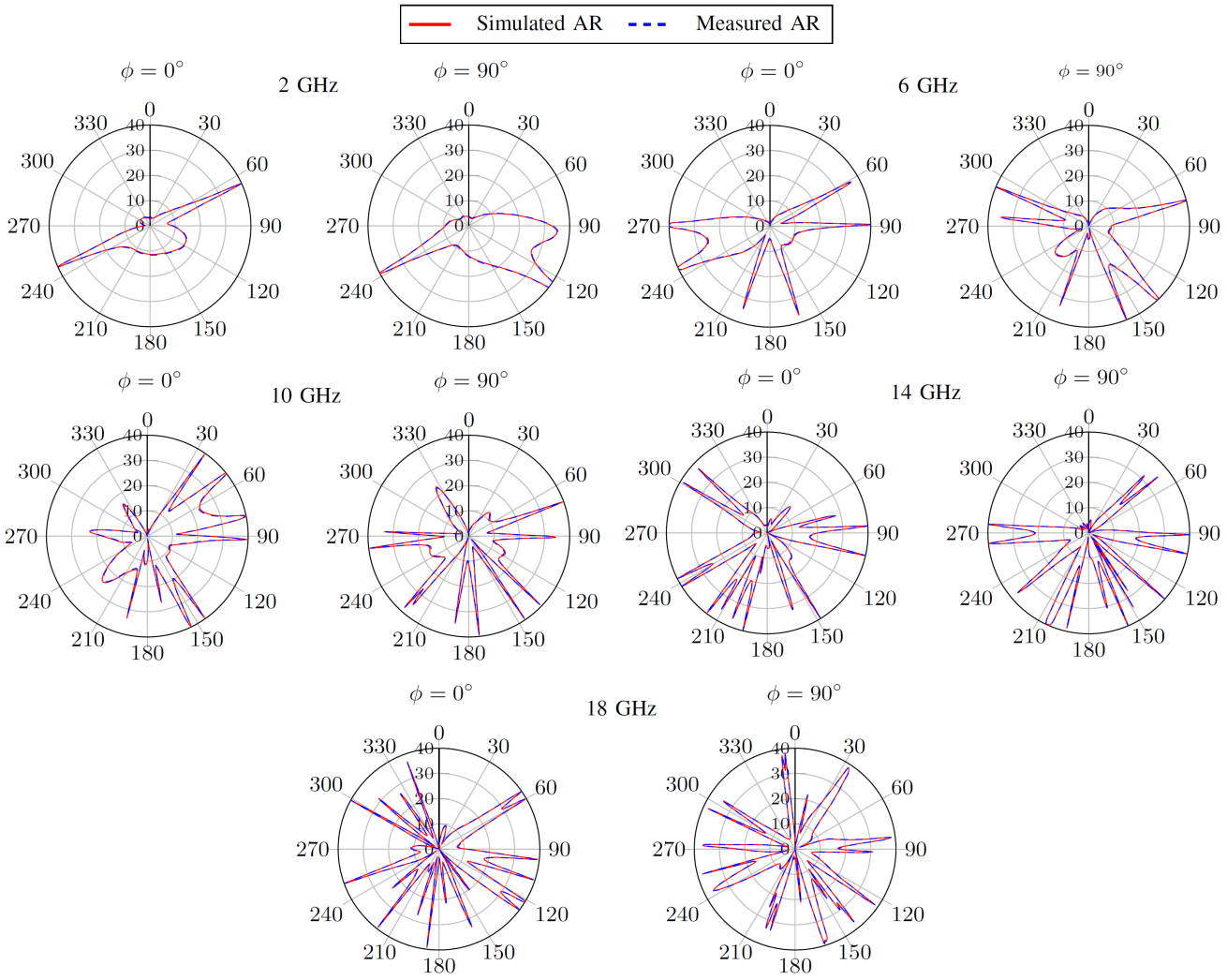

FIGURE 20. AR plot at $\phi = 0°$ and $\phi = 90°$ planes at different frequencies.

is considered, because other works report only the bare antenna length without packaging.

TABLE 1. Comparison with reported works.

Ref.	λ_L (D)	H/λ_L	Freq. (GHz)	Gain dBic	AR < 3 (GHz)
[13]	0.40	0.33	2–18	−3–4	2–18
[14]	0.33	0.45	2–18	−9.31–4	2–18
[15]	0.33	0.21	2–18	−4.9–2	2–18
[16]	0.35	0.14	2–18	−2–5	2.30–18
[17]	0.37	0.31	2–18	−6–4	3–18
[18]	1.34	0.20	3–11	−2–6	3–10
[19]	0.43	N.A	2.5–17.5	−10–8	2.5–17.5
P.W.	0.46	0.10	2–18	0.1–10	2.15–18

P.W. = Proposed Work, N.A. = Not Available

4. CONCLUSION

A compact spiral antenna with a bent planar feed was designed, fabricated, and tested at 2–18 GHz. The measured results closely matched those of the simulations, validating the proposed design. The modified feed improved both the gain and axial ratio compared with conventional reference feeds. Moreover, integrating the feed ground with the reflector ground reduces the antenna height and overall size by approximately 55–60% without compromising the return loss, gain, or polarization performance. The inclusion of a tapered microstrip balun enables a low-profile, wideband, circularly polarized structure, making it suitable for electronic countermeasure (ECM) applications such as radar warning receivers, missile systems, and EW pods, where compactness and integration are critical. Overall, the proposed design provides a practical, high-performance solution for modern EW systems.

REFERENCES

[1] Sachs, J., *Handbook of Ultra-Wideband Short-Range Sensing: Theory, Sensors, Applications*, John Wiley & Sons, 2013.

[2] Dyson, J., "The equiangular spiral antenna," *IRE Transactions on Antennas and Propagation*, Vol. 7, No. 2, 181–187, Apr. 1959.

[3] Turner, E. M., "Spiral slot antenna," Aerial Reconnaissance Laboratory, WADC, Technical note WCLR 55-8, Project 4341, Jun. 1955.

[4] Gebeşoğlu, D., M. Kuloğlu, A. O. Ertay, and S. Şimşek, "Low-profile closed cavity backed spiral antennas with circular AMC reflector for V/UHF bands," *AEU — International Journal of Electronics and Communications*, Vol. 170, 154861, 2023.

[5] Sağ, R. N., T. Tüylü, and N. T. Tokan, "Comparison of size reduction techniques in spiral antenna design," in *2023 33rd International Conference Radioelektronika (RADIOELEKTRONIKA)*, 1–6, Pardubice, Czech Republic, 2023.

[6] Mashaal, O. A., S. K. A. Rahim, A. Y. Abdulrahman, M. I. Sabran, M. S. A. Rani, and P. S. Hall, "A coplanar waveguide fed two arm Archimedean spiral slot antenna with improved bandwidth," *IEEE Transactions on Antennas and Propagation*, Vol. 61, No. 2, 939–943, 2013.

[7] Sharma, C. and D. K. Vishwakarma, "Miniaturization of spiral antenna based on Fibonacci sequence using modified Koch curve," *IEEE Antennas and Wireless Propagation Letters*, Vol. 16, 932–935, 2017.

[8] Zhong, Y.-W., G.-M. Yang, J.-Y. Mo, and L.-R. Zheng, "Compact circularly polarized archimedean spiral antenna for ultrawideband communication applications," *IEEE Antennas and Wireless Propagation Letters*, Vol. 16, 129–132, 2017.

[9] Eubanks, T. W. and K. Chang, "A compact parallel-plane perpendicular-current feed for a modified equiangular spiral antenna," *IEEE Transactions on Antennas and Propagation*, Vol. 58, No. 7, 2193–2202, Jul. 2010.

[10] Lestari, A. A., E. Bharata, A. B. Suksmono, A. G. Yarovoy, and L. P. Ligthart, "Bent tapered microstrip balun transformer," in *2009 Asia Pacific Microwave Conference*, 2156–2159, Singapore, 2009.

[11] Mahalakshmi, B. N., S. Singh, K. A. Ajith Kumar, and C. Viswanadham, "Effect of feed line bend on the performance of spiral antenna," in *2022 IEEE Microwaves, Antennas, and Propagation Conference (MAPCON)*, 856–860, Bangalore, India, 2022.

[12] Balanis, C. A., *Frequency Independent Antennas and Antenna Miniaturization*, 3rd ed., 545–550, Wiley, 2009.

[13] Akkaya, E. and F. Güneş, "Ultrawideband, high performance, cavity-backed Archimedean spiral antenna with phelan balun for direction finding and radar warning receiver applications," *International Journal of RF and Microwave Computer-Aided Engineering*, Vol. 31, No. 5, e22596, 2021.

[14] Durbha, R. and M. N. Afsar, "Miniaturization techniques using magnetic materials for broadband antenna applications," *IEEE Transactions on Magnetics*, Vol. 55, No. 7, 1–7, Jul. 2019.

[15] Ali, A., M. Hamza, and W. T. Khan, "Smallest form factor, high performance 2–18 GHz cavity-backed archimedean spiral antenna," in *2017 International Symposium on Antennas and Propagation (ISAP)*, 1–2, Phuket, Thailand, 2017.

[16] Rahman, N. and M. N. Afsar, "A novel modified archimedean polygonal spiral antenna," *IEEE Transactions on Antennas and Propagation*, Vol. 61, No. 1, 54–61, Jan. 2013.

[17] Seong, C. M. and D. C. Park, "Design of cavity-backed spiral antennas," in *Proceedings of 2012 5th Global Symposium on Millimeter-Waves*, 186–190, Harbin, China, 2012.

[18] Tanabe, M. and H. Nakano, "Low-profile wideband spiral antenna with a circular HIS reflector composed of homogenous fan-shaped patch elements," *IEEE Transactions on Antennas and Propagation*, Vol. 68, No. 10, 7219–7222, Oct. 2020.

[19] Afsar, M. N., Y. Wang, and D. Hanyi, "A new wideband cavity-backed spiral antenna," in *IEEE Antennas and Propagation Society International Symposium. 2001 Digest. Held in conjunction with: USNC/URSI National Radio Science Meeting (Cat. No.01CH37229)*, Vol. 4, 124–127, Boston, MA, USA, 2001.

[20] Klopfenstein, R. W., "A transmission line taper of improved design," *Proceedings of the IRE*, Vol. 44, No. 1, 31–35, Jan. 1956.

[21] Wu, C.-H., C.-H. Wang, and C. H. Chen, "Novel balanced coupled-line bandpass filters with common-mode noise suppression," *IEEE Transactions on Microwave Theory and Techniques*, Vol. 55, No. 2, 287–295, Feb. 2007.

[22] Micronics, J. V., "Flat multilayer broadband absorber jvmbf226," [Online]. Available: www.jvmicronics.com, 2025.

[23] "Dassault Systèmes, CST Studio Suite 2021," Computer Simulation Technology, 2021.